A&A 404, 883–899 (2003)
DOI: 10.1051/0004-6361:20030508

Astronomy & Astrophysics

An optical imaging study of $0.4 \leq z \leq 0.8$ quasar host galaxies[⋆,⋆⋆]

I. Observations and reduction

E. Örndahl, J. Rönnback, and E. van Groningen

Department of Astronomy and Space Physics, Uppsala University, Box 515, 751 20 Uppsala, Sweden

Received 24 February 2003 / Accepted 1 April 2003

Abstract. We have conducted an optical imaging study aimed at resolving the host galaxies of 79 radio-loud and radio-quiet quasars at $z = 0.4-0.8$, extending the number of investigated objects in this redshift range by ∼45%. Observations were performed mainly in the *R* band but also in *V* and *I* band using the Nordic Optical Telescope on La Palma. In this paper we discuss the sample composition and observations and the reduction techniques used. The quasars were selected in pairs of radio-loud and radio-quiet objects matched in the *z*–*V* plane in order to facilitate a statistical comparison. The radio-loud part of the sample contains comparable numbers of flat and steep radio spectrum sources which also are matched in redshift and *V* magnitude. Point spread function subtraction was performed using one-dimensional luminosity profiles both on the quasar image and on a field star, and subtracted images and luminosity profiles are shown for each quasar field. The detection rate is 60% for the radio-quiet host galaxies and 80% for radio-loud hosts. The host galaxies have magnitudes which make them brighter than an L^* galaxy by a factor of 1.5–4 at the low end of the redshift range, which increases by 2–3 times towards the higher end of the redshift range. Both radio-quiet and radio-loud hosts follow the radio galaxy *R*–*z* Hubble relation well. Analysis and discussion of colours and morphology is presented in Örndahl & Rönnback (2003).

Key words. galaxies: active – quasars: general – galaxies: fundamental parameters – galaxies: photometry

1. Introduction

The properties of quasar host galaxies are of fundamental importance in that they further our understanding of the AGN phenomenon. By studying the hosts, clues to the origin and fuelling of the AGN may be provided and the subset of the galaxy population which is capable of producing and sustaining high nuclear activity defined. Such studies can also help constrain physical models of quasar evolution and provide insight on the links between the growth of supermassive black holes and the formation of galaxies.

Using both ground-based instruments as well as the Hubble Space Telescope (HST), investigations of quasar host galaxies at low redshifts have in recent years yielded a wealth of information, both in the optical and near-infrared. The hosts of luminous quasars all seem to be bright galaxies having a luminosity $>L^*$ (Taylor et al. 1996; Bahcall et al. 1997; McLeod & McLeod 2001), but the early indications of a host galaxy morphology determined by radio-loudness in the sense that radio-loud quasars (RLQ) reside in early-type galaxies and radio-quiet quasars (RQQ) in spiral hosts (Smith et al. 1986; Hutchings et al. 1989) have been superseded by a picture in which the nuclear luminosity determines the morphology so that only massive spheroidals can host AGNs above a certain luminosity limit (McLure et al. 1999; Dunlop et al. 2003). In addition, a correlation has been found between the luminosities of nearby quasars and those of their host galaxies (McLeod & Rieke 1995; Hooper et al. 1997). Studies at low redshift have furthermore revealed that the relation between bulge luminosity and black hole mass found for nearby galaxies holds also for host galaxies (Magorrian et al. 1998; Laor 1998) but with an apparent offset between the masses of the black holes powering RLQ and RQQ which grows with increasing redshift (McLure et al. 1999; Laor 2000; Kukula et al. 2001).

Host galaxies at higher redshifts are increasingly difficult to resolve and also suffer from rapid cosmological surface brightness dimming of the host in contrast to the nucleus. The similarity between the strong evolution of the quasar population with redshift and the rate of galaxy formation has driven a

Send offprint requests to: E. Örndahl, e-mail: eva@astro.uu.se

⋆ Based on observations made with the Nordic Optical Telescope, operated on the island of La Palma jointly by Denmark, Finland, Iceland, Norway, and Sweden, in the Spanish Observatorio del Roque de los Muchachos of the Instituto de Astrofísica de Canarias.

⋆⋆ Only part of Appendix A is presented in printed format, but can be found in its entirety at http://www.edpsciences.org

wide interest in host galaxies at $z > 1$ in an effort to uncover the connections between nuclear activity and host properties (e.g. Heckman et al. 1991; Aretxaga et al. 1998; Lehnert et al. 1999). The hosts of RLQ have brightened considerably more than RQQ hosts by $z \simeq 2$ (Kukula et al. 2001; Falomo et al. 2001; Ridgway et al. 2001), perhaps indicating pronounced differences between the two categories of host galaxy.

In contrast, host galaxies in the intermediate redshift range (corresponding to a look-back time of around 3.5−5.5 Gyr) have not been as extensively investigated. Apart from the occasional few objects entering the tail end of a sample targetting low ($z \lesssim 0.5$) or high ($z \gtrsim 0.9$) redshift or being sources of special interest (as e.g. Véron-Cetty & Woltjer 1990; Brotherton et al. 1999), not many dedicated surveys have been carried out. The earliest such studies were performed in the optical (Romanishin & Hintzen 1989; Hutchings et al. 1989) but later authors have concentrated on near-infrared imaging so as to achieve larger host flux ratios relative to the nucleus (Carballo et al. 1998; Márquez et al. 1999, 2001; Kotilainen et al. 1998; Kotilainen & Falomo 2000), with the exception of the HST *R* band study of 16 RLQ and RQQ in the interval $0.4 < z < 0.5$ by Hooper et al. (1997). The results are consistent with the findings at low redshift: the hosts are similar to or brighter than an L^* galaxy and obey the correlation between host and quasar luminosity in that more powerful quasars reside in more luminous hosts.

The sample presented in this paper constitutes the main part of our investigation of RLQ and RQQ in the redshift interval $0.4 \leq z \leq 0.8$, the first part of which was published in Rönnback et al. (1996) (hereafter R96). We aim to compare the properties of the host galaxies of RLQ and RQQ found at the less well explored intermediate redshifts, in order to discern possible differences between the two host classes and to link the results obtained at low redshift to those at high redshift. Since previous studies in this interval mainly have concentrated on RLQ while the by far most common quasar type is radio-quiet, we have constructed a sample composed of equal numbers of RLQ and RQQ matched in magnitude and redshift.

The R96 sample is comprised of 23 objects which to date is the largest uniform survey available in the intermediate redshift range. These hosts are luminous, with a difference between the magnitudes of RLQ hosts and RQQ hosts of only 0.3 mag (corresponding to 1.5σ). Furthermore, the colours obtained from *R*, *V* and Gunn *i* indicate host galaxies as blue as late-type spirals or irregular galaxies. In this paper an additional 79 objects are presented, increasing the collected total number of investigated sources at intermediate redshifts by ∼45%. Imaging in *R*, *V* and *I* band was carried out using the Nordic Optical Telescope under favourable seeing conditions.

The layout of this paper is as follows. In Sect. 2 the sample properties are discussed, with special attention given to the possible influence the several emission lines entering the optical broadband filters may have (Sect. 2.3). Section 3 details the observations and in Sect. 4 the reduction process and the process of point spread function (PSF) subtraction are addressed. The derived host galaxy properties are presented in Sect. 5 and discussed in Sect. 6, and in Appendix A we show images and luminosity profiles of the sample quasars and their host galaxies. The full analysis of the complete sample including the R96 data will be published in Örndahl & Rönnback (2003) (Paper II), where the colours of the host galaxies and morphological considerations will be discussed.

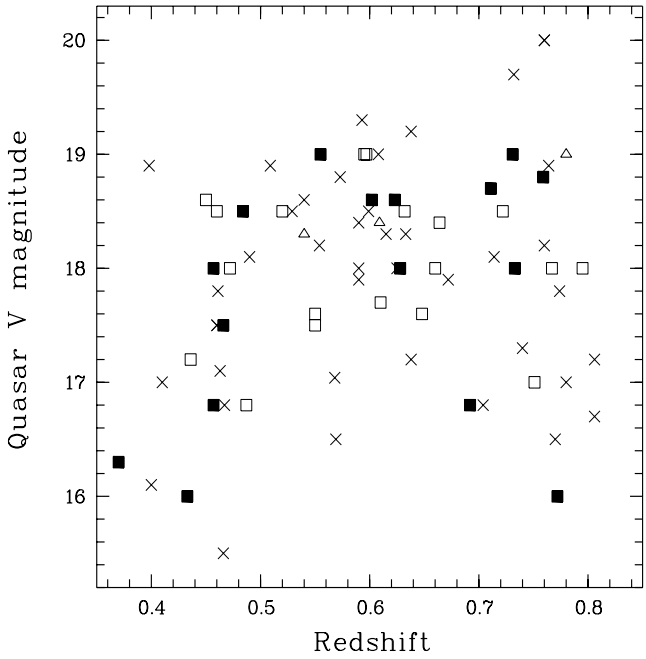

Fig. 1. Redshifts and apparent *V* magnitudes of the sample quasars. Radio-quiet quasars are marked by crosses, flat spectrum radio-loud quasars and steep spectrum radio-loud quasars by open squares and filled squares respectively. Non-classified radio-loud quasars are marked with a triangle.

Throughout this paper we adopt an Einstein-de Sitter universe ($q_0 = 0.5$) and a Hubble constant of $H_0 = 75$ km s^{-1} Mpc^{-1}.

2. Sample selection and properties

2.1. Sample composition

The sample was selected from the catalogues of Véron-Cetty & Véron (1993) and Hewitt & Burbidge (1993), where the selection criteria used were the redshift range ($0.4 \leq z \leq 0.8$) and the constraints imposed by the sky coordinates at the observation site. To ensure that the radio-loud and radio-quiet subsamples were drawn from the same distribution in the *z*–*V* plane, matched pairs of RLQ and RQQ with approximately the same redshift and apparent *V* magnitude were selected in order to make a direct statistical comparison between the two classes easier (as in e.g. Hutchings et al. 1989 and Dunlop et al. 1993). A two-dimensional Kolmogorov-Smirnov test confirms that no statistically significant difference exists between the two subsamples in this respect.

The sample of 79 quasars is presented in Table 1 and Fig. 1. The values of $L_{5\,\mathrm{GHz}}$, the *V* magnitude and the redshift have been updated with current data from the NASA/IPAC Extragalactic Database (NED). We use the criterion for radio-loudness from Kellermann et al. (1989), namely a luminosity

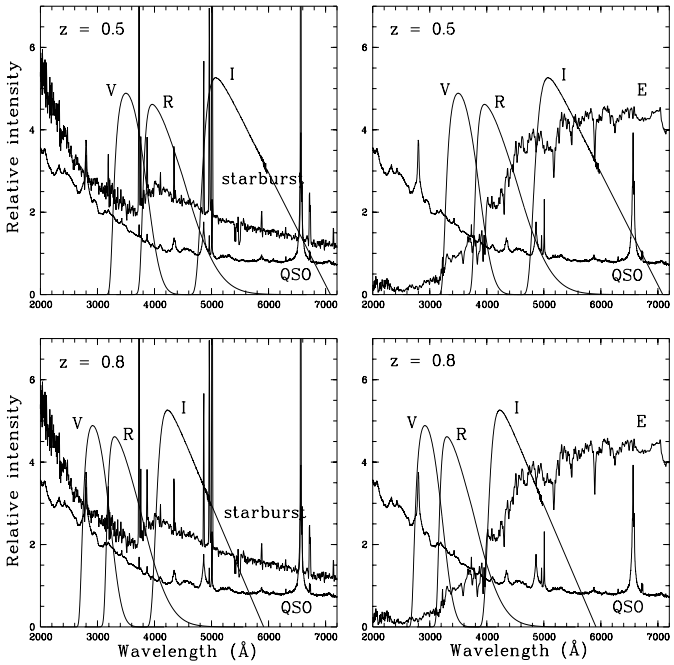

Fig. 2. Position of the filter profiles at $z = 0.5$ and $z = 0.8$. We use template galaxy spectra from Kinney et al. (1996) and the composite quasar spectrum from Vanden Berk et al. (2001). The intensity scales are arbitrary.

of $L_{5\ \mathrm{GHz}} > 2.5 \times 10^{24}\ h_{100}^{-2}$ W Hz^{-1}, which for our assumed cosmology translates into $L_{5\ \mathrm{GHz}} > 4.5 \times 10^{24}$ W Hz^{-1}.

2.2. Radio loudness

Observations of the quasar radio luminosity function have shown it to be of a bimodal nature (Kellermann et al. 1994; Miller et al. 1993), where a wide gap separates the radio-loud from the radio-quiet objects. There is however a class of objects termed radio-intermediate quasars (Miller et al. 1993; Falcke et al. 1996) which have radio luminosities falling between these two principal groups. The radio-intermediate quasars are possibly intrinsically radio-quiet objects with a jet-producing central engine where the radio emission has been relativistically boosted along the line of sight (Falcke et al. 1996) or, depending on the possible existence and size of associated extended lobe emission, they may be RLQ of very low luminosity (Kukula et al. 1998). Using the VLA FIRST survey (Becker et al. 1995), recent work by White et al. (2000) on the other hand shows it to be likely that the radio emissivity is not a discontinuous property so that radio-selected quasars instead occur at all levels of radio-loudness. The quasars in our sample, however, neatly fall into a bimodal distribution and published radio luminosities for our objects do not indicate that any radio-intermediate quasars have been included.

A more thorough investigation has been performed by Wold et al. (2001) for their sample of RQQ at $0.5 \leq z \leq 0.8$. They examine the 1.4 GHz NVSS (Condon et al. 1998) and the VLA FIRST survey for detections of their objects, calculate the flux density at 5 GHz and find that out of 20 RQQ, only three have luminosities that surpass the limit for radio-quietness. Thus, these objects are better classified as radio-intermediate. Likewise, Kukula et al. (1998) detect two such sources when determining the radio properties of their sample of 27 RQQ at low redshift ($z < 0.3$). We therefore conclude that even though a few of the radio-quiet sources in our sample have no available radio flux measurements, the likelihood that their emission in radio is strong enough to make them radio-intermediate is small.

Radio-loud quasars can be subdivided into flat spectrum (FS) and steep spectrum (SS) sources, with different properties. Flat spectrum quasars exhibit rapid variability and have high and variable polarization. Their radio emission is core-dominated and they more often display superluminal motion than the lobe-dominated SS quasars, which in the unified scheme is explained by SS objects having a larger viewing angle between the radio axis and our line of sight (e.g. Urry & Padovani 1995). During the sample selection process the radio-loud objects were not monitored for radio spectral index α. Subsequent calculation of the spectral indexes (setting the division between FS and SS objects at $\alpha_{2.7}^{5} = 0.5$) shows that this resulted in a blind draw of 16 FS and 20 SS sources. Three objects could not be classified. Investigating the two subsets of RLQ with a two-dimensional Kolmogorov-Smirnov test gives the result that their distributions in the z–V plane do not differ significantly and thus that the radio-loud subsample in itself is matched in terms of spectral index.

2.3. Emission line properties

When selecting the sample, no adjustment was made for the effect of emission lines entering the filters at different redshifts. In Fig. 2 we plot the position of our filter profiles at different redshifts, together with a composite quasar spectrum obtained from the SDSS (Vanden Berk et al. 2001) and template spectra for an elliptical galaxy and a starburst galaxy (Kinney et al. 1996).

As can be seen, both the [OIII]λ5007 and Hβ emission lines are present in the wing of the R filter (crossing below the half power point of the R band at $z \simeq 0.5$), and affect the I filter throughout the observed redshift range. Likewise, the [OII]λ3727 emission line passes out of the V band wing at $z \simeq 0.7$ and lies within the R filter profile for all of the sample. Flux contributions from these strong emission lines could therefore influence the derived host galaxy magnitudes and colours. The lines can be produced in star formation regions in the host galaxy itself and in extended emission line envelopes, and can also be present due to scattered light from the quasar.

2.3.1. Young stars

The ionization of gas by young stars gives rise to strong emission in the Balmer lines as well as in [OIII]λ5007 and [OII]λ3727, but only during a period of some few times 10 Myr after the initial star formation event. The inclusion of these lines in our filters makes our observations more sensitive

to host galaxies with a pronounced young stellar population than to early-type host galaxies.

Still, the host galaxies of lower redshift quasars seem to be if not almost exclusively of elliptical type (Dunlop et al. 2003), then at least predominantly so (Schade et al. 2000). Spectroscopical studies of low-redshift samples ($z \lesssim 0.2$) also show a very small contribution from younger stellar populations to the host galaxy light, typically less than 1% by mass from a 0.1 Gyr old component (Nolan et al. 2001; Jahnke et al. 2001). At higher redshifts, the host galaxies still have properties consistent with them being drawn from a population of inactive field galaxies, preferentially massive ellipticals. The luminosity profiles of the hosts of both RLQ and RQQ also follow a Kormendy relation similar to that of giant massive ellipticals (Kotilainen et al. 1998; Kotilainen & Falomo 2000; Kukula et al. 2001).

There are a few exceptions to the rule, though. Blue colours were found for the host galaxies in R96, and also in the three radio-loud host galaxies with $0.35 \leq z \leq 0.6$ studied by Kirhakos et al. (1999). Furthermore, Brotherton et al. (1999) have discovered a quasar at $z = 0.634$ with spectral features suggesting a starburst event only 400 Myr old, which may have an even younger component (Brotherton et al. 2002), but which in any case is too old to display any [OII]λ3727 emission. While the additional uncertainties which may be introduced should be kept in mind, we assume that in general the contribution of light to the emission lines in our filters caused by young stars in the host galaxy is small.

2.3.2. Emission line envelopes

The emission lines in question can also be produced in an extended narrow line region or emission envelope ionized by the quasar nucleus. Since the quasar spectrum extends to very high energies heavy ions dominate the opacity. As a result the Hβ line strength is considerably lower than that of [OIII]λ5007: a ratio of [OIII]/H$\beta > 10$ is not unusual. For this reason Balmer emission lines will be regarded as insignificant and we will concentrate on the contribution that the forbidden oxygen lines make to the host galaxy magnitudes.

Stockton & MacKenty (1987) found extended nebulosities in [OIII]λ5007 for somewhat less than half of their sample of quasars at $z < 0.5$, mainly around steep spectrum RLQ. Of their objects with $z > 0.35$, six sources (35% of the sample), all steep spectrum, had envelopes. Hes et al. (1996) have conducted an emission-line imaging study of steep spectrum RLQ in [OII]λ3727 at intermediate redshifts, and have also compiled literature data on additional objects. Since the [OII] line has much lower critical density for de-excitation it is expected to be radiated at larger radii than [OIII].

In the work by Crawford & Vanderriest (1997, 2000) on steep spectrum RLQ in the same redshift interval as our sample, the [OIII] and [OII] envelopes have similar sizes within the detection limits. In either case the diameters of these envelopes cover the same range as those determined by Hes et al. (15–25 kpc), and are consistent with more recent findings for host galaxies at both intermediate and high redshifts where the line emission is either compact and well inside the body of the host galaxy (Márquez et al. 1999; Kirhakos et al. 1999; Hutchings et al. 2001) or not detected at all (Aretxaga et al. 1998; Lehnert & Becker 1998), though Stockton & Ridgway (2001) find [OII]λ3727 emission around a quasar at $z = 1.2$ which clearly is compact but distributed quite differently than the light in the K band. It should also be noted that a few extreme cases exist where the emission envelopes are of more than double the size quoted here.

About half of the objects imaged by Hes et al. show extended nebulosities, with a mean total luminosity in [OII]λ3727 for the quasars of $\log L_{[\mathrm{OII}]} = 35.5$ W. This coincides with the value obtained by Crawford & Vanderriest who also estimate the mean contribution made by only the emission envelope to the line luminosity to be $\log L_{[\mathrm{OII}]} = 35.0$ W. The [OIII]λ5007 luminosities are higher, with a mean value for the envelope part of $\log L_{[\mathrm{OIII}]} = 35.9$ W. Computing the mean magnitude of the [OII]λ3727 line and comparing it to the mean R magnitude of our sample reveals a contribution from the line of less than 0.05 mag to the host galaxy magnitude, even when the line is centered in the filter. For the V band images the line contribution is of similar size. The [OIII]λ5007 line exerts a larger influence and supplies in the worst-case scenario an additional $\simeq$0.3 mag to the mean I magnitude. For individual objects the line can of course play a much less significant role, depending on the redshift of the object and on whether an envelope even exists. Corrections to the host magnitudes to compensate for possible emission line envelopes are further addressed in Sect. 5.2.

2.3.3. Scattered quasar light

A third possible contribution to the emission lines entering the filters can be made by scattered light from the quasar nucleus itself. The scattering can occur either by electrons, in which case no change in the colour of the light will take place, or by dust, which for an inhomogeneous dusty medium with opaque dust scattering clouds again results in grey scattering (Witt & Gordon 1996, 2000; Városi & Dwek 1999). The importance of scattered quasar continuum light in general is discussed in more detail in Sect. 6.1. Here we note that comparisons of radio galaxies and RLQ result in an estimate for the fraction of scattered light from the central source of about 10% (Fosbury 1997). With a typical quasar luminosity in [OII]λ3727 of $\log L_{[\mathrm{OII}]} = 35.3$ W and in [OIII]λ5007 of $\log L_{[\mathrm{OIII}]} = 36.2$ W (Crawford & Vanderriest 2000), the amount of scattered light entering the filters from the oxygen lines is much less than 0.1 mag and can thus be considered insignificant.

The mean value of the quasar Hβ luminosity has been found to be $\log L_{\mathrm{H}\beta} = 36.6$ W from comparison of relative fluxes in Vanden Berk et al. (2001). Therefore, scattered light from the quasar Hβ line can contribute more than 5% of the host galaxy flux when the line is centered in the R or I band filter. In addition, the Hα line is passing out of the I band at the low end of the redshift range investigated here, but being the brightest Balmer line it still can contribute around a tenth of a magnitude.

The Mg II emission line is however not strong enough to affect the V band, since the line only begins to enter the filter for the highest redshifts in our range. Corrections for scattered line emission will be further addressed in Sect. 5.2.

3. Observations

The main part of the observations were performed during two runs of ten nights each in June respectively October 1994 at the 2.56 m Nordic Optical Telescope (NOT) on La Palma. For the June 1994 run we used a Thomson 1024×1024 CD, kindly on loan from the Instituto de Astrofísica de Canarias, with a pixel scale of 0.″14/pixel. During the October 1994 run the detector used was the Brorfelde TEK 1024 × 1024 CCD, with a pixel scale of 0.″18/pixel. A few additional fields were obtained at the NOT in December 1998, using the ALFOSC 2k Loral CCD with pixel scale 0.″188/pixel.

All quasars were observed in the R band. To keep the core unsaturated we obtained for each object a series of three to five dithered exposures of 300 to 500 s, giving a total integration time of in most cases 2000 s. For 24 objects where an indication of a host galaxy was seen (either by eye in the raw frames or in coadded images combined on site) we also performed observations in V and/or I, with integration times of typically two to four times 500 to 700 s. Standard star fields from Landolt (1992) were taken throughout the nights during all runs. The data obtained is almost entirely of photometric quality – only a few objects observed in October could not be calibrated, and most of these were subsequently calibrated with frames taken during the December run.

A summary of the observations is presented in Table 1, where the $FWHM$ is calculated from the coadded frames. The median seeing value for the coadded frames is less than 0.″85, with 15% of the frames having a seeing better than 0.″55. There is no significant difference in seeing between radio-loud and radio-quiet frames if the December data (which suffered from much poorer seeing conditions and mainly targeted radio-quiet objects) is excluded. This also holds for the SS and FS radio-loud subsamples.

For a handful of quasars we encountered various problems. The objects US 3150 and 4C 09.72 were saturated (thus rendering PSF subtraction impossible), and the object OU 401 was accidentally placed on a bad column in the CCD. Furthermore, ZC 2354+002 has a very uncertain redshift determination, and the position of 1951+4950 coincides very closely with that of a field star so that no PSF subtraction was possible. These five objects were thus excluded from the sample.

4. Data reduction and analysis

4.1. Reduction

The reduction of the raw CCD frames followed standard procedures and was carried out with the ESO MIDAS package.

We first subtracted bias and corrected for bad columns, then flattened each science frame using either twilight skyflats or superflats obtained from stacks of typically ten dithered science images normalized to the sky. The dithered images of each object were then aligned to an accuracy of ~0.05 pixels and combined to a master frame, in order to increase the signal to noise and permit efficient removal of artifacts, bad pixels and cosmic hits. Finally, the combined frames were photometrically calibrated. When an object or object field is referred to henceforth in this paper, it is the coadded frame which is implied.

All reduced frames were flat to less than 0.2%. The photometric calibration of the object frames was accomplished via aperture photometry on each standard star, with an uncertainty in the photometric zero points measured to be 0.03 mag. The photometric error due to sky variations is less than 0.04 mag for a source brighter than 21 mag, except for the more sensitive I band where the error is less than 0.04 mag for a source of less than 20 mag and below 0.08 mag for a source brighter than 21 mag. For a few objects from the October run the images obtained were of non-photometric quality; however, additional photometric calibration observations were carried out in December 1998.

Some of the sources in the sample were observed on multiple occasions. When such was the case, we chose to use the observation with superior image quality, either due to lower seeing or being the deeper exposure. For some objects the double observations are of very similar quality, in which case we analysed both fields and computed the mean magnitude, thus obtaining a single magnitude value for each object.

4.2. PSF construction

The data has been analysed using two different methods for determining the PSF in each image: a purely empirical one and a PSF constructed from a combination of empirical and model data.

The advantage of using a noise-free model PSF is that no extra noise is added in the PSF subtraction thus making it possible to reach fainter levels of host galaxy flux, but in frames where the core part of the PSF is slightly non-circular the empirical PSF is difficult to model. When constructing the combined PSF, we therefore retained the high-signal empirical core but replaced the low-signal wings by a noise-free model. The model used is the profile from Saglia et al. (1993), which provides a better fit to stellar profiles than either a Gaussian or a Moffat function. The composite PSF was used to good advantage in R96, and for further details of the construction method we refer to this paper.

In each object frame we chose a field star to use for constructing the empirical PSF. An optimal star is one whose intensity is comparable to or higher than that of the quasar, so that this source of noise contribution to the residual image from the subtraction process is minimised. When possible, we chose a star close to the object to eliminate effects on the residual from variations of the PSF over the field: however, the $FWHM$ of the PSF is stable to within 1−2% over the field.

We first rebinned the star to pixel center and next performed background subtraction, where the sky level was determined from star-free regions well away from the objects. The centering was checked again and azimuthally averaged luminosity

Table 1. General properties and observation summary of the sample quasars.

Object	α (1950)	δ (1950)	V	z	$L_{5\ \mathrm{GHz}}$ (10^{26} W Hz^{-1})	Integration time (s)			Date	$FWHM$ (arcsec)
						R	V	I		
0007+0236	00 07 45	02 36 57	18.4	0.59	–	2000			Oct. 05	0.85
							2100		Dec. 09	1.31
								1000	Oct. 05	0.89
0010+0146	00 10 01	01 46 45	18.0	0.59	–	2000†			Oct. 06	1.12
0015+1612	00 15 56	16 12 47	18.2	0.554	–	2000			Oct. 04	0.77
0020–0300	00 20 21	−03 00 57	17.3	0.58	–	2000†			Oct. 06	1.13
0021–0100	00 21 38	−01 00 25	18.2	0.77	–	2000‡			Oct. 09	0.97
0058+0205	00 58 59	02 05 47	18.5	0.599	–	2000			Oct. 04	0.78
							2100		Dec. 09	1.45
								2000‡	Oct. 09	0.68
0110+0125	01 10 50	01 25 57	17.8	0.774	–	2000			Oct. 05	1.11
1E 0112+3256	01 13 00	32 56 48	18.9	0.764	–	2000			Dec. 07	2.64
PKS 0130+2412	01 30 39	24 12 19	16.8	0.457	1.29	1900†			Oct. 06	1.17
PHL1072	01 35 12	05 40 12	18.3	0.615	–	2000			Oct. 05	0.86
1E 0136+0606	01 36 20	06 06 50	18.5	0.450	0.21	2500‡			Oct. 11	0.75
								1500‡	Oct. 12	1.08
KUV 0200–0858	02 00 57	−08 58 12	16.5	0.77	–	2000‡			Oct. 09	0.77
MC 0212+1708	02 11 59	17 08 52	18.0	0.472	1.71	2000‡			Oct. 12	1.07
5C 6.189	02 15 45	31 35 39	19.0	0.597	0.60	2000‡			Oct. 11	0.63
EX 0240+0044	02 40 06	00 44 43	16.5	0.569	–	1500⋆			Oct. 04	0.82
						2000			Dec. 10	1.81
							2400		Dec. 10	2.07
US3150	02 44 18	−01 12 04	16.8	0.467	–	2000⋆			Oct. 09	0.65
0256+0140	02 56 14	01 40 29	19.0	0.608	–	2000			Oct. 05	0.81
US3605	03 01 48	00 10 53	17.2	0.638	–	2000			Oct. 04	0.78
0305+0222	03 05 38	02 22 56	17.9	0.59	–	1500			Oct. 05	0.90
							2100‡		Oct. 11	0.77
								1800	Dec. 10	1.96
PKS 0353+0247	03 53 22	02 47 43	19.0	0.602	2.60	1000			Oct. 05	0.87
							700‡		Oct. 09	0.77
							2400‡		Oct. 11	0.87
								2400	Dec. 09	1.31
3C 138	05 18 16	16 35 27	18.8	0.759	59.6	2000			Oct. 04	0.67
MC 0657+1740	06 57 37	17 40 08	18.5	0.722	1.67	1600			Oct. 05	0.81
							550‡		Oct. 11	0.88
B2 0709+3701	07 09 47	37 01 14	15.7	0.487	1.14	1400⋆			Oct. 04	0.74
						2000			Dec. 08	1.38
GC 0742+3321	07 42 46	33 20 54	17.7	0.610	1.03	2000			Dec. 08	1.04
								2400	Dec. 09	1.20
LB 0847+1905	08 47 39	19 05 02	16.6	0.568	–	2000			Dec. 08	1.71
0929+5319	09 29 13	53 19 53	19.0	0.595	3.24	2100			Dec. 10	1.04
MC 1157+1150	11 57 12	11 50 31	19.0	0.731	0.87	900			June 13	0.87
						1500			June 14	0.60
1240+1551	12 40 30	15 51 37	18.8	0.573	–	500			June 14	0.56
						1000			June 15	0.75
3C 275.1	12 41 27	16 39 18	19.0	0.555	7.04	2000			June 09	0.88
							3500		June 10	0.69
								2400	June 16	0.57
1242+1719	12 42 52	17 19 32	18.6	0.54	–	2000			June 11	1.04
CSO179	12 50 53	31 22 07	16.7	0.78	–	2200			June 15	0.59
AB122	13 03 22	33 51 34	18.1	0.49	–	3000			June 17	0.53
W23694	13 06 07	30 21 39	17.2	0.806	–	2000			June 12	0.78
E 1332+3730	13 32 00	37 30 55	18.2	0.438	–	1500			June 12	0.86
							1700		June 14	0.54
								2200	June 16	0.56

Table 1. continued.

Object	α (1950)	δ (1950)	V	z	$L_{5\ \mathrm{GHz}}$ (10^{26} W Hz^{-1})	Integration time (s) R	V	I	Date	$FWHM$ (arcsec)
TEX 1423+1438	14 23 25	14 38 26	19.0	0.78	12.7	2000			June 13	1.21
							2400		June 17	0.61
								2400	June 16	0.49
1435+0130	14 35 24	01 30 52	18.3	0.633	–	2000			June 11	1.03
PG 1443+1015	14 43 54	10 15 44	19.7	0.732	–	2000			June 10	0.73
1446+0218	14 46 05	02 18 55	17.9	0.672	–	2000			June 13	1.02
PKS 1451+0946	14 51 27	09 46 34	18.5	0.632	3.12	2000			June 11	0.96
B2 1512+3701	15 12 46	37 01 55	15.5	0.37	1.10	2000			June 17	0.71
							1000		June 17	0.68
							1400		June 18	0.67
PKS 1530+1342	15 30 54	13 42 28	19.0	0.711	5.34	2400			June 14	0.52
PG 1538+4745	15 38 00	47 45 15	16.0	0.772	0.62	2000			June 09	0.89
PG 1543+4855	15 43 59	48 55 30	16.1	0.40	–	2000			June 15	0.60
							3000		June 15	0.55
								2400	June 16	0.47
MC 1548+1129	15 48 21	11 29 47	17.2	0.436	1.99	1500			June 10	0.87
MC 1608+1123	16 08 11	11 23 16	18.0	0.457	0.62	2000			June 12	0.83
1631+3757	16 31 19	37 57 19	19.2	0.638	–	2000			June 11	0.89
OS 562	16 37 17	57 26 16	17.0	0.751	25.5	2000			June 09	0.89
1637+3910	16 37 35	39 10 48	17.8	0.461	–	2000			June 11	0.82
MS 1640+3940	16 40 06	39 40 42	18.3	0.540	0.35	2000			June 12	0.92
1640.5	16 40 29	39 44 13	18.0	0.625	–	2000			June 13	0.99
						500			June 15	0.52
1641.7	16 41 45	39 58 46	16.8	0.705	–	2000			June 10	0.73
								2400	June 16	0.53
1641+3959	16 41 53	39 59 18	19.3	0.593	–	2000			June 12	1.10
							3000		June 14	0.60
B2 1657+2634	16 57 22	26 34 03	18.0	0.795	8.84	2000			June 10	0.72
4C 45.34	17 05 50	45 40 02	17.6	0.648	4.72	2200			June 09	0.97
						1000			June 17	0.50
								1000	June 17	0.50
B2 1724+3959	17 24 54	39 59 32	18.	0.66	3.26	2000			June 13	0.91
B2 1752+3528	17 52 04	35 28 29	17.5	0.55	0.36	2000			June 12	1.09
						2000			June 14	0.61
							3000		June 15	0.55
								2400	June 16	0.47
OU 401	18 00 03	44 04 18	17.5	0.663	12.2	1000			June 09	0.92
PKS 1819+2249	18 19 07	22 49 46	18.	0.628	3.13	2000			June 12	0.79
4C 40.37	18 19 13	40 50 12	18.	0.733	2.87	1500			Oct. 05	1.07
4C 56.27	18 23 15	56 49 18	18.4	0.664	12.3	2000			June 13	0.87
							1400		June 18	0.74
								2000	June 18	0.61
3C 380	18 28 13	48 42 40	16.8	0.692	57.2	2000			June 11	1.01
						1500			June 16	0.53
							2800		June 11	1.08
								2500	June 13	0.79
1951+4950	19 51 12	49 50 24	17.5	0.466	1.06	2000			June 10	0.77
							2800		June 17	0.59
								1200	June 16	0.50
								1000	June 17	0.56
MS 2037–0035	20 37 21	−00 35 20	18.4	0.609	0.20	2000			June 12	0.73
PG 2112+0555	21 12 23	05 55 12	15.5	0.466	–	2000			June 09	0.93
2112+0556	21 12 49	05 56 02	18.9	0.398	–	2000			Oct. 05	0.95
2113+0536	21 13 39	05 36 05	18.9	0.509	–	2400‡			June 14	0.72
2141+0402	21 41 52	04 02 38	17.1	0.463	–	1500			June 09	1.06
						1200			June 14	0.74

Table 1. continued.

Object	α (1950)	δ (1950)	V	z	$L_{5\ \mathrm{GHz}}$ (10^{26} W Hz^{-1})	Integration time (s)			Date	$FWHM$ (arcsec)
						R	V	I		
MC 2142+1101	21 42 52	11 01 36	17.6	0.550	2.58	2000			June 13	0.99
							1200		June 13	0.99
								2000	June 15	0.52
MG2149	21 47 06	07 42 24	18.5	0.52	2.70	1500			June 10	0.86
PKS 2209+0804	22 09 32	08 04 25	18.5	0.484	4.16	1500			June 10	0.76
						1500			Oct. 04	0.72
							2800‡		Oct. 09	0.89
								2000‡	Oct. 09	0.68
2217+0845	22 17 42	08 45 24	18.6	0.623	1.12	1500			June 11	1.06
						1500			Oct. 04	0.70
							2100		June 17	0.60
								1500	June 16	0.48
								1500	Oct. 04	0.70
2232+1316	22 32 06	13 16 30	20.0	0.760	–	2000			Dec. 09	1.15
2235+0054	22 35 00	00 54 58	18.5	0.529	–	1500			June 15	0.74
2238+0133	22 38 19	01 33 45	18.1	0.714	–	2000			Oct. 04	0.74
						2000			Dec. 10	2.39
PKS 2247+1315	22 47 16	13 15 16	18.	0.767	9.82	2000			Oct. 04	0.69
						500			Oct. 05	0.75
								2000	Oct. 05	0.74
4C 09.72	23 08 46	09 51 57	16.0	0.433	1.06	2200⋆			Oct. 05	0.89
2350–0236	23 50 18	−02 36 58	17.5	0.46	–	1000†			Oct. 09	0.88
PKS 2351–0036	23 51 35	−00 36 30	18.5	0.46	1.84	1500†			Oct. 12	0.73
ZC 2354+002	23 54 55	00 12 58	17.0	0.41	–	1500			Oct. 04	0.84

† Object observed during non-photometric conditions.
‡ Object observed during non-photometric conditions, but calibrated with data obtained in December 1998.
⋆ Quasar saturated.

profiles and growth curves were computed. The growth curves provide an extra control that the background has been correctly subtracted: when these curves did not show proper asymptotic behaviour the process was repeated. When necessary we performed masking of close companions, stars or other features which would give an unwelcome contribution to the luminosity profile.

4.3. PSF subtraction

In order to determine the magnitudes of the host galaxies, the nuclear and stellar light contributions must be disentangled. We have achieved this by subtracting a scaled PSF from the quasar images. Since the amount of flux originating from the point source itself is unknown, care is required in the choice of scaling factor. A subtraction to zero flux in the central pixels will remove all quasar light to a certainty, but also an unknown amount of host galaxy light. To minimise the oversubtraction of the host galaxy, we have chosen a scaling factor which results in a residual having a flat-top luminosity profile and positive flux at all radii. This monotonically decreasing residual is a more realistic representation of a real galaxy, but is still likely to be an oversubtraction for elliptical galaxies and spirals with a bulge since these have a peaked profile. The magnitudes we obtain will as a result be upper limits. As a first rough estimate of the scaling factor the PSF was normalized to the quasar and then subtracted. By utilising the luminosity profile of the resulting residual we iteratively arrived at a scaling factor which rendered the luminosity profile monotonous while at the same time ensuring that no negative pixels were present in the central parts of the host galaxy image.

There are cases when the two requirements of flat-top residual and non-negativity are incompatible. This can happen for a host galaxy which is off-centered from the quasar source but also when the central part of the PSF profile for some reason is broader than that of the quasar, either because the quasar is close to saturation or because of variability of the PSF shape over the CCD. In such cases we have relaxed the flat-top criterion from demanding that the flux in the two first luminosity profile points be equal, to accepting a slightly lower value for

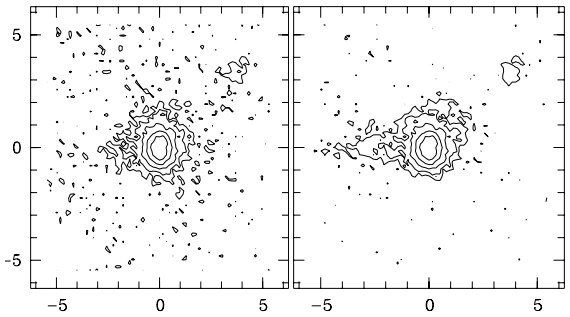

Fig. 3. Contour plots of the quasar KUV 0200−0858. To the left the residual after subtraction of the empirical PSF and to the right after subtraction of the combined PSF. North is up, east to the left. The contours mark the 21, 22, 23, 24 and 25 mag arcsec^{-2} levels and the image scale is in arcseconds.

the second point as long as the third point equals the first. This procedure as well as the slight resulting oversubtraction is acceptable as long as no large errors arise in the growth curves of these objects. The magnitudes obtained in this way have a larger uncertainty and have been marked in Tables 3 and 4. For eight fields, however, the second point in the profile deviated so much that a proper scaling factor (and consequently, host galaxy flux) could not be reliably determined, even after testing different PSF stars when such were available in the field. These fields were deselected from further analysis, leading to four objects falling out of the sample.

4.4. PSF evaluation

To independently check the PSF it was also subtracted from one or more field stars, since the residual in these cases should become negligible. This exercise was possible for all but seven fields (where there was no star other than the PSF star) and resulted in barely detectable stellar residues in most cases, proving the overall validity of the PSF.

For all objects we performed subtraction of both the empirical and the combined PSF. The difference between the two methods is only discernible in the very outermost parts of the host galaxy, where the composite PSF method detects very faint structures. The resulting total magnitudes are therefore very similar.

In Fig. 3 we show as an example the two different residuals for the quasar KUV 0200−0858. The model subtraction is less influenced by sky noise, and also uncovers a slight extension to the northwest. The extension towards the east is a low-level charge transfer streak which can be seen in the unsubtracted image. The presence of the streak is much less visible in the empirical subtraction due to the inclusion of this feature in the wings of the empirical PSF.

Unfortunately, the Saglia et al. models have circular luminosity profiles and do not allow for a proper treatment of ellipticity. In combination with the charge transfer problem noted above this has a serious impact on our attempts to determine the morphology of the host galaxies. These questions will be further discussed in Paper II, since only detections and magnitudes are addressed here, none of which depend on the method of subtraction. We will therefore present values from empirical subtractions alone. The images and luminosity profiles of the sample quasars and their host galaxies are presented in Fig. A.1.

4.5. Error estimation

There are a number of different errors that can contribute to the host galaxy magnitude estimation, divisible into two categories: the Poisson error in the subtraction method and the systematic error due to oversubtraction of the core component. The sizes of the photometric zeropoint errors have been measured to be quite small, as have also the uncertainties arising from determining the proper growth curve limit. Typically, the growth curve flattens at a surface brightness of ∼26 mag arcsec^{-2} for the R and V band images, and at ∼25 mag arcsec^{-2} in the I band, whereas the variation in sky level always was found to correspond to a surface brightness more than a magnitude fainter. Thus, uncertainties in the sky background are not a dominant source of error. By comparing the magnitude determinations made for stars in the field the photometric error was measured to be $\lesssim$0.1 mag. The influence of the PSF shape variation on the derived magnitude was investigated by choosing objects having several suitable PSF stars distributed over the field and performing the subtraction using all of these stars. The error obtained was found to be $\lesssim$0.1 mag.

Scaling and subtracting the PSF from stars in the field provides a check of how well the subtraction method performs. This control yielded a mean flux of the stellar residuals which is 7% ± 10% of the host galaxy flux derived for that field, placing them below 1σ of the Poissonian noise expected from the subtraction technique by combining the error sources dealt with above. The small size of this error is attributable to the overall high quality of the data and the instrumental setup.

To investigate the systematical oversubtraction error simulated host galaxies were created. A field star including background was added to an elliptical galaxy model which previously had been convolved by the model PSF which best fitted the stellar image used. Then PSF subtraction was carried out in the same way as for real data. This was done for a small set of point source and galaxy brightnesses and resulted in values very similar to those derived in R96, leading us to adopt that error determination as valid for the data set in this paper. For a galaxy magnitude of $R = 19$, the extracted host flux is less than the original one by an amount corresponding to 0.10±0.05 mag, while the difference for $R = 20$ and 21 mag is 0.20 ± 0.10 and 0.50 ± 0.10 respectively.

A further oversubtraction ensues in the case when a relaxed flat-top has to be adopted when determining the scaling factor (as discussed in Sect. 4.3). To control the size of this oversubtraction as well as the stability of the procedure itself, two of the authors have independently computed scaling factors for a subset of the object frames. As long as the requirements of flat-top residual and non-negativity were met the scaling factors differed by a negligible amount. However, in those instances when the flat-top criterion had to be relaxed the oversubtraction could increase by up to 0.1 mag, also increasing the spread in this error by about 0.03 mag. Thus, a more problematic

luminosity profile has a larger error than indicated in the simulations.

By comparing the magnitudes of the host galaxy residuals extracted from those objects for which we have multiple observations the accuracy of the PSF subtraction can be tested. The difference between residuals was measured to be ±0.2 mag but is the mean of a range of host galaxy magnitudes, whereas the size of the intrinsic error is expected to be larger for fainter hosts. The number of sources observed at more than one occasion are however too few to allow for a more finely tuned estimation of the differences. Brighter hosts will have magnitudes recoverable by subtraction with an error within 1σ of the total (Poisson plus intrinsic) error, whereas faint hosts or those where the flat-top criterion had to be modified have a less well-defined magnitude. Summing up, the error in the host galaxy magnitudes amounts to 0.25–0.3 mag, which is in the same range as error estimates compiled by other authors comparing objects observed on more than one occasion (Véron-Cetty & Woltjer 1990; Maraziti & Stockton 1994; Kotilainen & Falomo 2000; McLeod & McLeod 2001).

5. Host galaxy properties

5.1. Detections

Of the initially 79 objects, 70 remain for analysis after the deselection of saturated or otherwise observationally flawed objects and those for which a scaling factor could not be reliably determined (as in Sect. 4.3). Kolmogorov-Smirnoff tests however show that both the radio-loud and radio-quiet subsamples as well as the SS and FS radio-loud subsamples still are matched with respect to redshift and quasar V magnitude.

Two additional tests were performed on parts of the sample to help discriminate between detections and artifacts caused by the subtraction process. Scaling of the PSF to remove stars in the field was used to evaluate the quality of the PSF shape, and was carried out on all objects but the seven which had no other star than the PSF star in the field. When the test star remainder was substantial the host galaxy residual was compared to it, and in case the shapes were very similar the residual was classified as a non-detection. We found this to be the case for ten fields.

It is possible that the flat-top criterion may have created a spurious host galaxy detection, in particular when the residual is small and the morphology quite circular. To look into this possibility the test of subtracting the quasar to zero in the center was performed for most objects, since even after subtraction to zero an undisputed host galaxy should have sizeable flux. Thus, based on comparison of the obtained zero-residual both to the result from flat-top quasar subtraction and to the stellar residue, eleven circular cases were indeed concluded to be non-detections.

In this way we detected host galaxies in 28 RLQ (14 of which have steep spectra) and 21 RQQ, comprising 80% and 60% of the total number of respective sources. Of these, one of the radio-loud (TEX 1423+1438) and two of the radio-quiet (0256+0140 and 2141+0402) detections must be deemed marginal. Eight other objects have been marginally resolved in one wavelength band but are clearly visible in the other band(s) employed so that they without a doubt constitute a detection. On the whole, more than half of the objects imaged in more than one band (13 out of 23) are detected in all bands. The difference between the mean seeing of the radio-loud and the radio-quiet subsamples is very slight, as already pointed out in Sect. 3. Comparison of the mean seeing for the frames where we detect a host galaxy to the mean computed for frames where no detection is made shows that the detection rate stays at a mean of ∼70% regardless of whether the seeing is below 1″, below 0.″8 or below 0.″55.

Since the sample was investigated primarily in the R band regardless of source redshift, some early-type hosts may have escaped detection due to the shift of the 4000 Å break from R into I for redshifts above ≃0.7. As most of the energy of an early-type galaxy is emitted longwards of this break, such a host will be much better visible in the I band than in R. Indeed, the detection rate for RLQ falls off by ≃20% and for RQQ by all of ≃35% above this redshift limit. The radio-loud quasar TEX 1423+1438 at $z = 0.78$ is an excellent example of the principle: while imaged in all three bands, only the I band image shows a host galaxy though very faint structures may be guessed at in the other bands.

Almost all non-detections have been classified as such by comparison with the results from stellar subtraction: only for a handful of cases is the quasar residue unresolved and so faint as to be virtually non-existent. From the simulations performed in R96, the lower limiting host magnitude was found to be $R \geq 21.5$. In this sample, four hosts have magnitudes fainter than $R = 21$ and two are fainter than $R = 21.5$. Inspection of the residual images make it clear that the hosts with $R \leq 21.5$ are resolved, whereas the two even fainter objects only are marginally resolved. The upper limit to the host magnitude determined from the unresolved faint sources in this sample is $R \geq 21.8$.

The claim made by Bahcall et al. (1995) that a large fraction of quasar hosts have luminosities substantially less than L^* has been shown to be erroneous by subsequent reanalysis of the original data (McLeod & Rieke 1995; Bahcall et al. 1997) and new imaging (McLure et al. 1999). Given that all unresolved objects have redshifts where the 4000 Å break has moved out of the filter used for observation, the reason for our failure to resolve these hosts is most likely not that they are so faint as to be completely outshone by the quasar, but rather because we are sampling an unsuitable region in the host galaxy spectrum.

In the object 3C 380 we detect no host galaxy in the R band when investigating the centre of the image. However, there is an off-centered structure, coinciding with the optical synchrotron hotspots detected by de Vries et al. (1997) with HST. Observations in [OII]λ3727 suggest that the two knots are dominated by optical continuum light instead of emission lines (O'Dea et al. 1999). In spite of the non-detection in the R band the host galaxy is clearly discernible in the V and I band, as is the hotspot feature.

5.2. Magnitudes

The magnitudes for the detected hosts were extracted at growth curve limit and measured with the help of the luminosity profiles. For a few objects with double observations of very similar quality, the differences between the two magnitude measurements were below ±0.1 mag. Thus, for the objects B2 1512+3701 in *V* band, PKS 2209+0804 in *R* band, and 2217+0845 in *I* band, both fields were analysed and the mean of the magnitude used. Values for the Galactic extinction were taken from Schlegel et al. (1998) for all objects in the sample. Due to the lack of constraints on the internal extinction in the host galaxies no such correction was performed.

It is of interest to compare the quasar *V* magnitudes obtained by us to the *V* magnitudes found in catalogues and listed in Table 1. For the 18 quasars imaged in *V*, the difference between observed and previously measured values amounts to ±0.4 mag with a mean of +0.2 mag, but it is to be remembered that these values refer to different epochs and thus could be influenced by the intrinsic variability of the objects.

To compensate for the influence from possible emission line envelopes in [OIII]λ5007 as discussed in Sect. 2.3.2, we apply a generic magnitude correction using the mean envelope luminosity of log $L_{[\mathrm{OIII}]}$ = 35.9 W (Crawford & Vanderriest 2000). The correction is detailed in the upper part of Table 2 and is only made for steep spectrum radio-loud objects, since these are most prone to have extended emission line regions.

The sample is divided into three redshift intervals chosen to center around the approximate main and half power points of the *R* and *I* filters. However, only the two lowest redshift intervals are used since for the highest bin the [OIII] line is in practice outside the *R* filter and in *I* the only object afflicted is 3C380, for which individual data could be found. For this quasar the luminosity in [OIII] is log $L_{[\mathrm{OIII}]}$ = 36.6 W (Lawrence et al. 1996), leading to a correction of 0.08 mag in *I* when assuming an envelope contribution of ∼30% to the total luminosity (Crawford & Vanderriest 2000).

It was possible to find a value for the quasar luminosity also for the object 3C 275.1. Here, log $L_{[\mathrm{OIII}]}$ = 35.8 W (Jackson & Rawlings 1997) giving an envelope contribution in *I* of 0.08 mag, but negligible in *R*. Finally, the object B2 1512+3701 is known to have a very bright envelope in [OIII]. Using the value for its [OIII] luminosity derived by Crawford & Vanderriest (2000), we find that a correction of 0.41 mag is necessary in *R*.

The host magnitudes must also be corrected for scattered quasar light in the Balmer lines (Sect. 2.3.3). The brightness of a typical quasar in these lines has been calculated from the composite in Vanden Berk et al. (2001), and the assumption made that 10% of the light is scattered. The generic magnitude corrections are listed in the lower part of Table 2 and are applied to all sources imaged in the shown redshift and filter combinations.

The resulting magnitudes are presented in Tables 3 and 4. The mean *R* magnitude of the radio-loud subsample shifts by only 0.03 mag when applying the modifications from Table 2, whereas the mean *I* magnitude shifts to 0.16 mag fainter.

Table 2. Mean magnitude corrections to compensate for extended [OIII]λ5007 emission line envelopes (upper part of table) and scattered quasar Balmer emission (lower part of table). Also shown are the number of sources affected in each interval, excepting the objects for which individual corrections for [OIII] emission were made.

Emission line	*z*-range	filter	correction	# obj
[OIII]	0.37−0.53	*R*	0.14	2
[OIII]	0.37−0.53	*I*	0.15	1
[OIII]	0.54−0.67	*I*	0.31	2
Hα	0.40−0.51	*I*	0.12	4
Hβ	0.37−0.42	*R*	0.13	2
Hβ	0.58−0.73	*I*	0.13	9

The mean *I* magnitude of the radio-quiet subsample shifts to 0.13 mag fainter.

6. Results and discussion

6.1. The nature of the hosts

The detected residuals have luminosities which typically are 15−25% of that of the quasar nucleus. Inspection of the residual images rarely reveal any unambiguous morphological markers at these redshifts: possible explanations for the nature of the diffuse light thus include not only stellar light but also nebular continuum produced by ionized gas and scattered quasar light.

As has been shown earlier, the emission line contributions from envelopes ionized by the quasar are not much more than a tenth of a magnitude. The continuum emission from undiscovered extended envelopes is therefore probably too weak to contribute all of the detected host flux. Indeed, no prominent narrow emission lines are seen in any of the off-nuclear host galaxy spectra obtained by Hughes et al. (2000) at $0.1 \leq z \leq 0.3$, indicating the relatively unimportant fraction of light coming from an envelope.

Quasar light which is scattered from dust and/or electrons can make a substantial contribution to the continuum emission in the ultraviolet, as is well known from spectropolarimetric measurements of radio galaxies (Fabian 1989; Tadhunter et al. 1992; Cimatti et al. 1993). If the unification scheme for radio-loud AGN is correct then the same effects which operate in radio galaxies can also influence the observed distribution of extended light around RLQ.

The fraction of scattered nuclear continuum light was estimated by Fosbury (1997) to be ∼10% of the total quasar light, which would make the measured hosts spuriously brighter by around a magnitude. This effect will be more prominent at shorter wavelengths where the light from an older stellar population is dominated by that of the AGN, and thus becomes more important at $z > 0.5$ where the ultraviolet emission has moved into the *V* band. For the *R* band this happens at redshift >0.8. Furthermore, the polarimetric properties of a complete sample of radio galaxies at redshifts up to $z \leq 0.7$ have been investigated by Tadhunter et al. (2002), who find that only in 30% of the objects at $z > 0.4$ does the scattered light make a significant

Table 3. Apparent magnitudes of the radio-loud quasars and host galaxies. The hosts of the objects PKS 0130+2412⋆ and PKS 2351−0036 were also resolved but have not been included in the table due to not being calibrated. Colon signs mark a marginal detection and an asterisk a steep spectrum source.

Object	z	Quasar			Host galaxy		
		R	V	I	R	V	I
1E 0136+0606	0.450	18.61		18.00	19.5		18.9:
MC 0212+1708	0.472	19.97			20.6		
5C6.189	0.597	18.70			20.6		
PKS 0353+0247⋆	0.602	18.14	18.83	17.29	19.6	21.0	19.1
3C 138⋆	0.759	18.52			21.2		
GC 0742+3321	0.610	18.91		18.14	20.2		18.9
0929+5319	0.595	18.59			20.3		
MC 1157+1150⋆	0.731	18.61			20.4		
3C 275.1⋆	0.555	17.95	18.32	17.43	19.2	20.2	18.2:
TEX 1423+1438	0.78	19.31	19.43	18.84			19.9:
PKS 1451+0946	0.632	18.49			19.9		
B2 1512+3701⋆	0.37	16.17	16.33		19.3:	19.4	
PKS 1530+1342⋆	0.771	19.21			21.2		
PG 1538+4745⋆	0.772	15.45			18.9		
MC 1548+1129	0.436	18.50			20.4		
MC 1608+1123⋆	0.457	19.61			20.4		
MS 1640+3940	0.540	18.27			20.2		
PKS 1819+2249⋆	0.628	17.56			20.3		
4C 40.37⋆	0.733	18.00			20.1		
4C 56.27	0.664	18.23	18.86	17.52	20.5	21.2:	19.1
3C 380⋆	0.692	16.67	16.87	16.33		18.1	18.4
MC 2142+1101	0.550	18.15	18.43	17.47	19.6		18.2
MG2149	0.52	17.28			19.1		
PKS 2209+0804⋆	0.484	18.69	19.22	18.16	20.3	20.7	19.2
2217+0845⋆	0.623	18.61	18.80	18.20	20.4		19.6
PKS 2247+1315	0.767	18.85		18.54	20.9		20.6:

Table 4. Apparent magnitudes of the radio-quiet quasars and host galaxies. The hosts of the objects 0010+0146 and 0020−0300 were also resolved but have not been included in the table due to not being calibrated. Colon signs mark a marginal detection.

Object	z	Quasar			Host galaxy		
		R	V	I	R	V	I
0007+0236	0.59	18.56	19.15	18.06	19.4	20.3	18.7
0015+1612	0.554	18.41			19.8		
0058+0205	0.599	18.47	18.52	18.22	20.0	20.0	19.7
PHL1072	0.615	17.81			20.0		
KUV 0200–0858	0.77	17.12			19.8		
EX 0240+0044	0.569	16.00	16.05		18.3	18.3	
0256+0140	0.608	18.57			21.4:		
0305+0222	0.59	17.92	18.51	17.64	20.0	21.9:	19.1
AB122	0.49	17.70			19.5		
E 1332+3730	0.438	17.60	17.75	17.28		20.6:	18.8
1435+0130	0.633	18.25			20.6		
PG 1543+4855	0.40	16.02	16.32	15.82	18.1	20.0	18.8:
1640.5	0.625	19.85			20.7		
1641.7	0.705	17.95		17.70			20.4
1641+3959	0.593	19.33	19.57		19.6	21.6:	
2113+0536	0.509	19.24			20.2		
2141+0402	0.463	16.78			20.3:		
2235+0054	0.529	19.39			20.6		
2238+0133	0.714	17.85			20.5		

contribution to the UV excess. The applicability of this result to quasar host galaxies is however far from certain. Both spectroscopic and polarimetric observations are needed to disentangle how important the contribution of scattered quasar continuum light is in general as well as in the individual case.

Given the difficulties involved no attempts were made to correct for scattered quasar light or nebular continuum, but the additional possible uncertainties in the host galaxy magnitudes should be kept in mind. In general, though, the colours of the host galaxies as determined from annular apertures are redder than those of the quasars, suggesting a minor influence from light sources other than the host galaxy itself. We will in the following assume that the dominant source of extended light is stellar emission originating in the host galaxy.

6.2. Comparisons of host magnitudes

The host galaxies apparent R magnitudes have been plotted versus redshift in Fig. 4, together with the R–z Hubble relation for radio galaxies (O'Dea et al. 1996). Objects which were only marginally resolved have not been included in the plot. For comparison, the brightness of a field galaxy having a

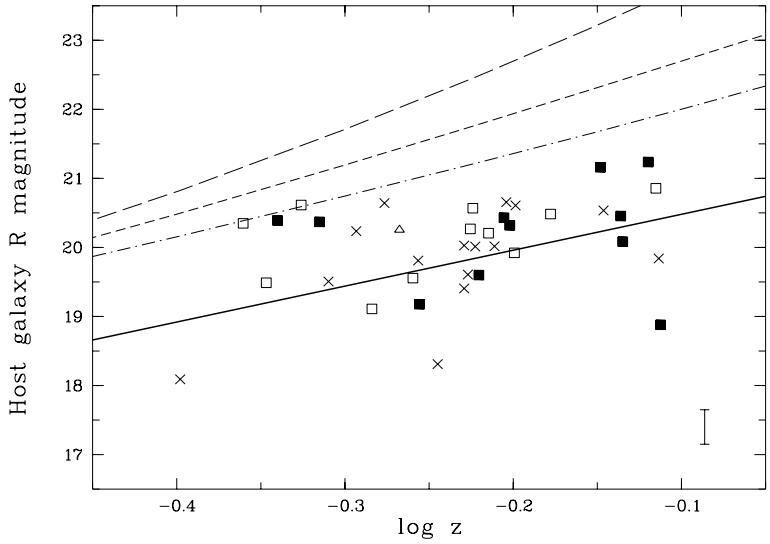

Fig. 4. The distribution of host galaxy *R* magnitudes with redshift. No marginally resolved objects have been included in the plot. Open squares mark flat spectrum radio-loud objects, filled squares steep spectrum radio-loud objects and triangles non-classified radio-loud objects. Radio-quiet objects are marked with crosses. The solid line is the Hubble *R–z* relation for radio galaxies (O'Dea et al. 1996). The long-dashed line shows the apparent magnitude of an L^* galaxy calculated using the *K*-correction from Fukugita et al. (1995) for an E galaxy. For the short-dashed line the Sbc galaxy type *K*-correction was used, while for the dash-dotted line the Im type *K*-correction was applied. The typical 2σ error in the host galaxy magnitudes is represented by the bar in the lower right corner.

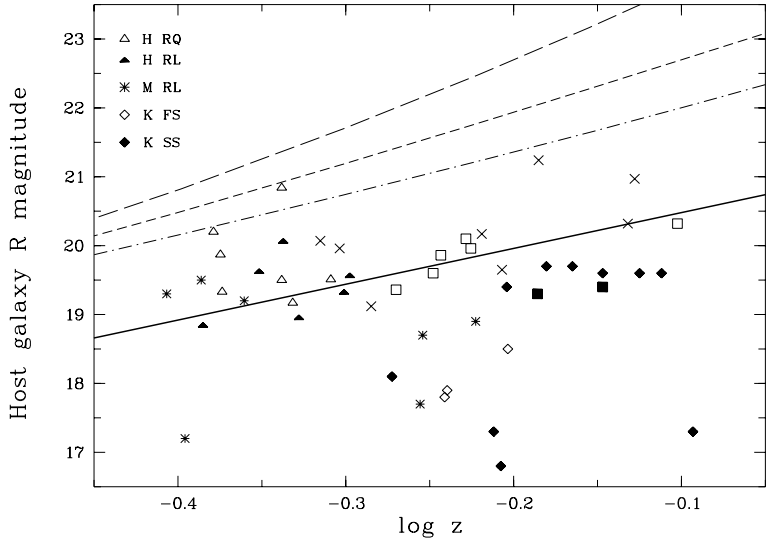

Fig. 5. The distribution with redshift of host galaxy *R* magnitudes from the literature. The lines are the same as in Fig. 4. Shown here is the R96 NTT data (symbols for radio-quiet, FS and SS radio-loud objects as in Fig. 4) and samples from Hooper et al. (1997), Márquez et al. (1999), Kotilainen et al. (1998) and Kotilainen & Falomo (2000), marked as indicated in the figure. Only resolved objects have been plotted.

characteristic (Schechter) magnitude of $M_{\mathrm{R}}{}^* = -20.9$ (Lin et al. 1996) has been plotted as well. To compute the corresponding apparent magnitude of the field galaxy, *K*-corrections appropriate for Hubble type E and Sc have been applied following the calculations of Fukugita et al. (1995).

The hosts follow the radio galaxy *R–z* relation, concurrent with the result for hosts at low as well as intermediate redshifts (Dunlop et al. 2003; Hooper et al. 1997; Márquez et al. 1999). Their luminosities are brighter than that of an L^* galaxy, and they also do not fade with redshift quite as rapidly as the field galaxy. At lower redshifts a simple least-squares fit to the data corresponds to 1.5−4 L^* depending on galaxy type, which increases to 2.5−12 L^* at the higher end of the redshift range. These values are consistent with the findings at redshifts of $\simeq$0.1−0.3, where the hosts of RLQ and RQQ are found to have luminosities ranging between 1−4 L^* (Dunlop et al. 2003, *R* band; Jahnke & Wisotzki 2000, *B* band; Boyce et al. 1998, *V* band; McLeod & Rieke 1994, *H* band), and also with the results from the intermediate redshift surveys by Kotilainen & Falomo (2000) and Kotilainen et al. (1998) who find a typical host luminosity of $\sim$6 L^* in the *H* band.

At redshifts above unity the luminosities of radio-loud hosts have increased by an amount well accounted for by passive evolution whereas the luminosities of radio-quiet hosts seem to be more or less unchanged, perhaps indicating less massive radio-quiet hosts at these redshifts (Kukula et al. 2001;

Falomo et al. 2001; Ridgway et al. 2001). It is not possible to discern any such trend towards the high end of the redshift range in the radio-quiet sample investigated here, as only three radio-quiet host galaxies were detected in R at a redshift larger than $z = 0.64$ (and of these, one source could not be calibrated).

In Fig. 5 we plot the R96 NTT data and samples from the literature (Hooper et al. 1997; Márquez et al. 1999; Kotilainen et al. 1998; Kotilainen & Falomo 2000). Only resolved objects having redshifts in the range 0.4−0.8 are shown (thus excluding the marginally resolved hosts from Kotilainen et al. and Kotilainen & Falomo, as well as from R96).

In the work of Hooper et al. magnitudes were determined both for an elliptical and a disk fit to the data. Here we use the magnitudes obtained for the elliptical fit (typically 0.5−1 mag brighter than those of the disk fit), thus assuming elliptical morphology for the host galaxies. The HST sample of Hooper et al. has been recalculated to R magnitude by the authors, whereas Márquez et al. have observed in J band and Kotilainen et al. in H band. Colour transformations were performed using $R - K = 2.5$, calculated by using $V - K = 3.9$ (Poggianti 1997) and $V - R = 1.44$ (Fukugita et al. 1995) for elliptical galaxy types. This $R-K$ value coincides with that found for both radio-loud and radio-quiet host galaxies at low redshift (Dunlop et al. 2003). Using values of $J - K$ and $J - H$ from Poggianti we find $R - J = 1.4$ and $R - H = 2.2$.

From Fig. 5 it is clear that the literature samples follow the radio galaxy R–z relation well, as already mentioned. The very bright hosts (mainly belonging to the Kotilainen et al. and Kotilainen & Falomo samples) are associated with brighter than average quasars, in accordance with the results from e.g. McLeod & Rieke (1995) that the minimum host galaxy luminosity increases with quasar luminosity. Comparing the host magnitudes shown in Fig. 4 to those in Fig. 5 reveals that the latter are somewhat brighter, at least toward the high end of the redshift range, which is not surprising given that the mean total magnitude of the sample investigated here is fainter at these redshifts than the objects collected from the literature.

To evaluate the possible difference between the R magnitude distributions with redshift of the radio-loud and radio-quiet host galaxies in our sample, a two-dimensional Kolmogorov-Smirnoff test was performed. The result shows that the two distributions are statistically indistinguishable (with a significance level of $p = 0.36$). There would thus seem to be no difference between the apparent magnitudes of radio-loud and radio-quiet hosts at the intermediate redshifts under study here, confirming and expanding the results of Hooper et al. (1997). A full analysis incorporating K-corrections is deferred to Paper II.

7. Summary

In this paper we have presented a sample of 79 radio-loud and radio-quiet quasars with redshifts of $0.4 \leq z \leq 0.8$ which were selected as matched pairs in the z–V plane. The radio-loud part of the sample also turned out to be matched in terms of spectral index. The quasars were imaged primarily in the R band but also in V and I band, using the Nordic Optical Telescope on La Palma.

PSF subtraction was performed with the help of one-dimensional luminosity profiles both on the quasar image and on a field star, to better control the quality of the subtraction. Host galaxies were detected in a total of 49 objects, corresponding to a 60% detection rate for radio-quiet hosts and an 80% detection rate for radio-loud hosts.

Apparent magnitudes are presented for the host galaxies and compared to a field galaxy having a Schechter luminosity as well as to the R–z Hubble relation for radio galaxies. The hosts are brighter than an L^* galaxy by a factor of 1.5−4 at the low end of the redshift range (depending on galaxy type), which increases to 2.5−12 L^* towards the higher end of the redshift range. They are found to follow the radio galaxy relation, regardless of whether they harbour a radio-loud or a radio-quiet quasar.

In Paper II we will include the data from R96 and analyse and discuss absolute magnitudes, colours and morphological considerations of the full sample of host galaxies.

Acknowledgements. The Instituto de Astrofísica de Canarias is gratefully acknowledged for lending us the CCD used during the June 1994 run. This research has made use of NASA's Astrophysics Data System Abstract Service, and also of the NASA/IPAC Extragalactic Database (NED) which is operated by the Jet Propulsion Laboratory, California Institute of Technology, under contract with the National Aeronautics and Space Administration.

Appendix A: Quasar host images and profiles

In Fig. A.1 we show images and luminosity profiles of selected quasars and their host galaxies, presented in order of right ascension. All fields shown in the printed version were taken in R band. The full set of images and profiles for the sample can be found in the electronic version of the article at EDP Sciences[1].

For each object field we present five plots. In the leftmost graph the luminosity profile is plotted (in mag arcsec^{-2}) versus radius in arcseconds. The points mark the quasar profile, the full-drawn line is the PSF, and the dotted line the residual after PSF subtraction. In the fourfold greyscale plot the image sizes are always $12\farcs5 \times 12\farcs5$ (except for the case of EX 0240+0044, where it is $20'' \times 20''$), with the objects always centred in the plots. Top left shows the host galaxy residual, top right is the unsubtracted quasar frame and in the bottom right graph we show the residual left from the scaling of the PSF to a field star. The bottom left graph is a contour plot of the host galaxy residual, where the number inside the plot denotes the value of the lowest contour in mag arcsec^{-2} and the spacing between contours is 1 mag arcsec^{-2}. The contours have been smoothed by a 3×3 box for better clarity of low-intensity features. North is up and east is to the left.

In the electronic version we in addition show fields observed in V or I band, where the luminosity profile has been labelled also with the filter name. Non-calibrated objects have been indicated by a #-symbol, and plots where we present a quasar residual subtracted to zero in the center in order to highlight the non-detection of a host galaxy have been marked with "zero".

[1] http://www.edpsciences.org

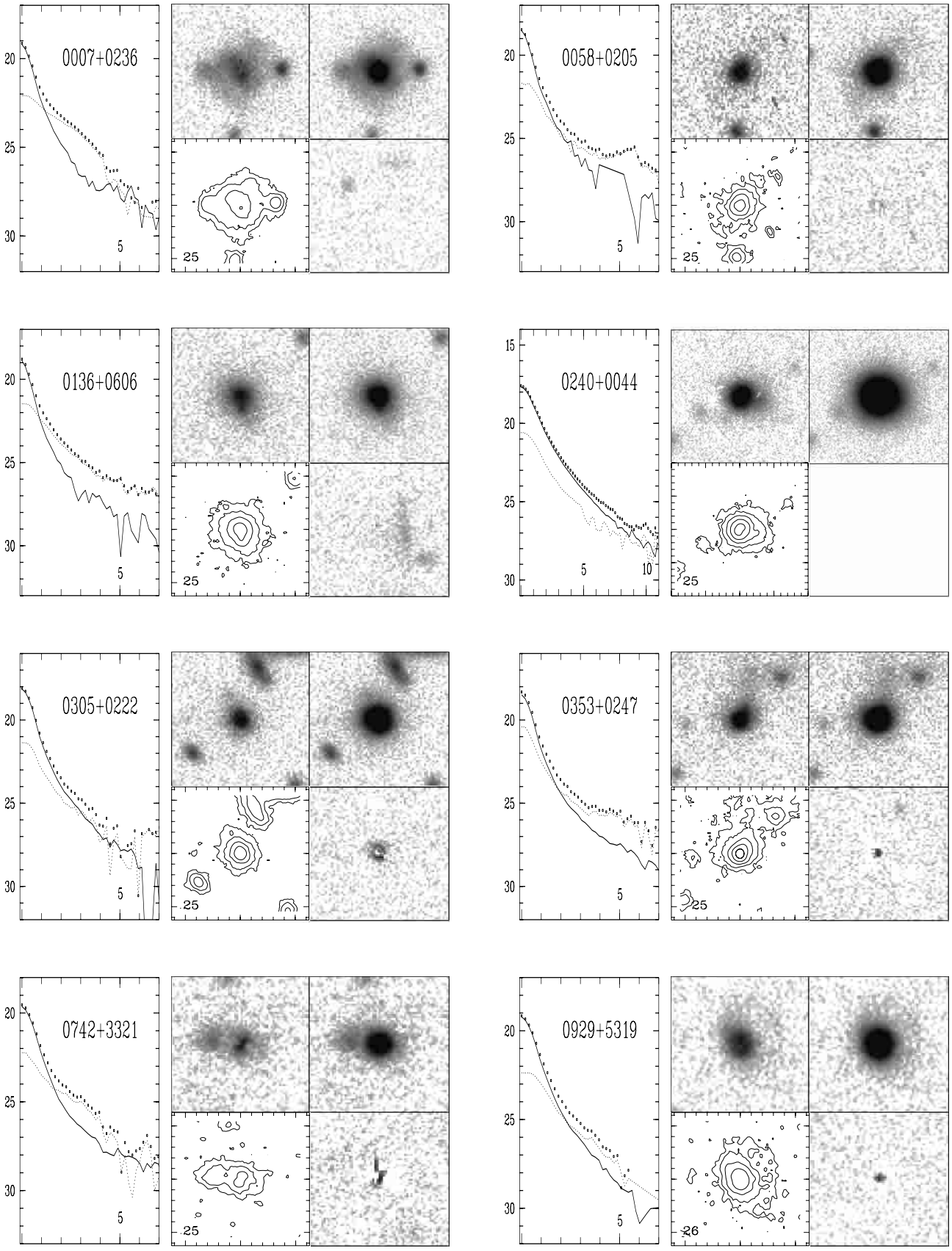

Fig. A.1. For each object field we present the luminosity profile in mag arcsec^{-2} with radius in arcsec (points: quasar profile, full-drawn line: PSF, dotted line: residual); centered greyscale images of residual (top left), unsubtracted quasar (top right) and test star remainder (bottom right); contour plot of the residual (number inside frame is lowest contour level in mag arcsec^{-2}, spacing of contours is 1 mag arcsec^{-2}). The image sizes are 12.″5 to a side, except for EX 0240+0044, where it is $20'' \times 20''$. North is up and east is to the left.

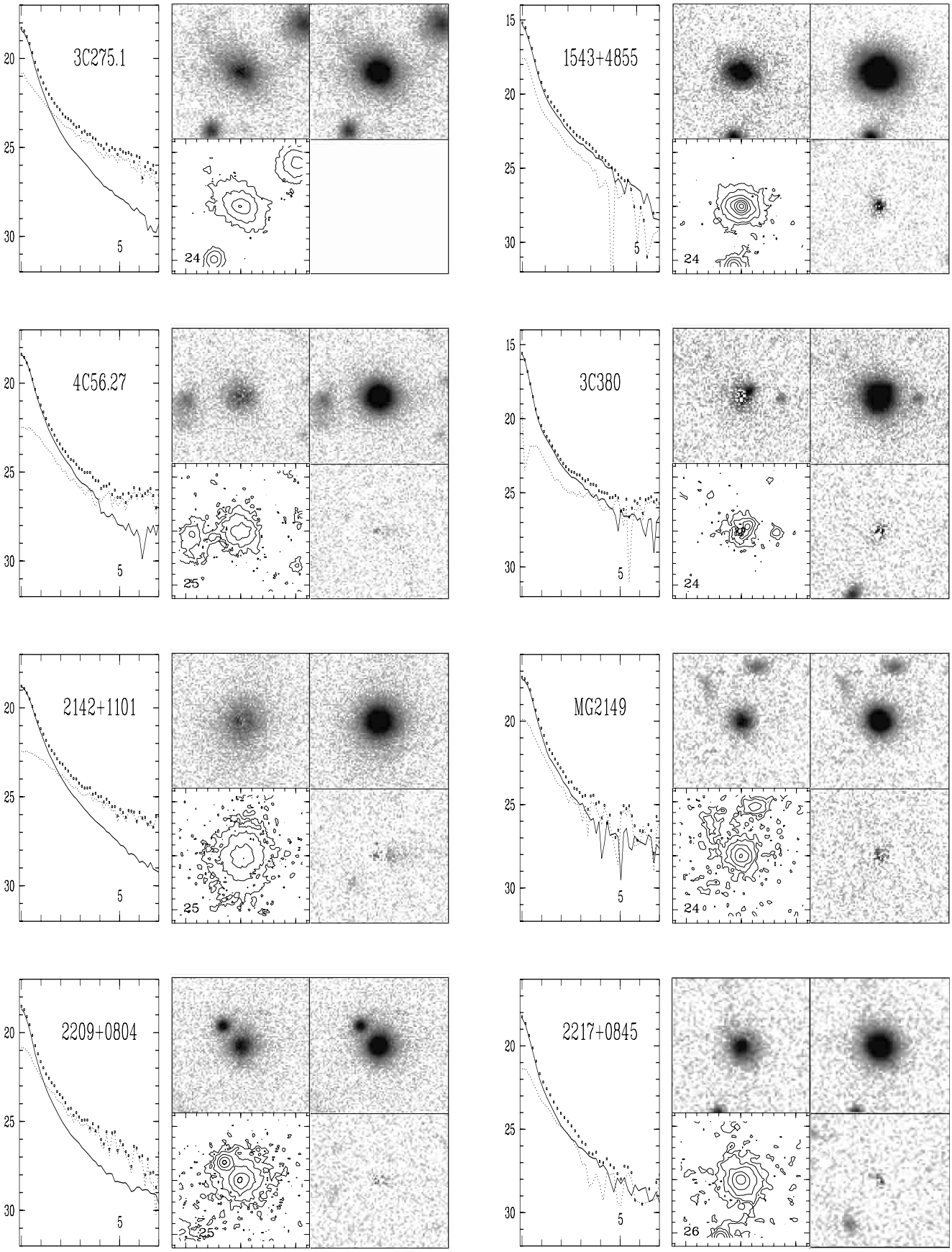

Fig. A.1. continued.

References

Aretxaga, I., Terlevich, R. J., & Boyle, B. J. 1998, MNRAS, 296, 643
Bahcall, J. N., Kirhakos, S., Saxe, D. H., & Schneider, D. P. 1997, ApJ, 479, 642
Bahcall, J. N., Kirhakos, S., & Schneider, D. P. 1995, ApJ, 450, 486
Becker, R., White, R. L., & Helfand, D. J. 1995, ApJ, 450, 559
Boyce, P. J., Disney, M. J., Blades, J. C., et al. 1998, MNRAS, 298, 121
Brotherton, M. S., Grabelsky, M., Canalizo, G., et al. 2002, PASP, 114, 593
Brotherton, M. S., van Breugel, W., Stanford, S. A., et al. 1999, ApJ, 520, L87
Carballo, R., Sánchez, S. F., González-Serrano, J. I., Benn, C. R., & Vigotti, M. 1998, AJ, 115, 1234
Cimatti, A., di Serego-Alighieri, S., Fosbury, R. A. E., Salvati, M., & Taylor, D. 1993, MNRAS, 264, 421
Condon, J. J., Cotton, W. D., Greisen, E. W., et al. 1998, AJ, 115, 1693
Crawford, C. S., & Vanderriest, C. 1997, MNRAS, 285, 580
Crawford, C. S., & Vanderriest, C. 2000, MNRAS, 315, 433
de Vries, W. H., O'Dea, C. P., Baum, S. A., et al. 1997, ApJS, 110, 191
Dunlop, J. S., McLure, R. J., Kukula, M. J., et al. 2003, MNRAS, 340, 1095
Dunlop, J. S., Taylor, G. L., Hughes, D. H., & Robson, E. I. 1993, MNRAS, 264, 455
Fabian, A. C. 1989, MNRAS, 238, 41
Falcke, H., Sherwood, W., & Patnaik, A. R. 1996, ApJ, 471, 106
Falomo, R., Kotilainen, J., & Treves, A. 2001, ApJ, 547, 124
Fosbury, R. 1997, in Quasar Hosts, ed. D. L. Clements, & I. Pérez-Fournon, ESO Conf. Ser., 3
Fukugita, M., Shimasaku, K., & Ichikawa, T. 1995, PASP, 107, 945
Heckman, T. M., Miley, G. K., Lehnert, M. D., & van Breugel, W. 1991, ApJ, 370, 78
Hes, R., Barthel, P. D., & Fosbury, R. A. E. 1996, A&A, 313, 423
Hewitt, A., & Burbidge, G. 1993, ApJS, 87, 451
Hooper, E., Impey, C., & Foltz, C. 1997, ApJ, 480, 95
Hughes, D. H., Kukula, M. J., Dunlop, J. S., & Boroson, T. 2000, MNRAS, 316, 204
Hutchings, J. B., Janson, T., & Neff, S. G. 1989, ApJ, 342, 660
Hutchings, J. B., Morris, S. L., & Crampton, D. 2001, AJ, 121, 80
Jackson, N., & Rawlings, S. 1997, MNRAS, 286, 241
Jahnke, K., Kuhlbrodt, B., Örndahl, E., & Wisotzki, L. 2001, in QSO Hosts and Their Environments, ed. I. Márquez, J. Masegosa, A. del Olmo, et al. (Kluwer Academic/Plenum Publishers), 89
Jahnke, K., & Wisotzki, L. 2000, MNRAS, submitted
Kellermann, K. I., Sramek, R., Schmidt, M., Shaffer, D. B., & Green, R. 1989, AJ, 98, 1195
Kellermann, K. I., Sramek, R. A., Schmidt, M., Green, R. F., & Shaffer, D. B. 1994, AJ, 108, 1163
Kinney, A. L., Calzetti, D., Bohlin, R. C., et al. 1996, ApJ, 467, 38
Kirhakos, S., Bahcall, J. N., Schneider, D. P., & Kristian, J. 1999, ApJ, 520, 67
Kotilainen, J. K., & Falomo, R. 2000, A&A, 364, 70
Kotilainen, J. K., Falomo, R., & Scarpa, R. 1998, A&A, 332, 503
Kukula, M. J., Dunlop, J. S., Hughes, D. H., & Rawlings, S. 1998, MNRAS, 297, 366
Kukula, M. J., Dunlop, J. S., McLure, R. J., et al. 2001, MNRAS, 326, 1533
Landolt, A. U. 1992, AJ, 104, 340
Laor, A. 1998, ApJ, 505, L83
Laor, A. 2000, ApJ, 543, L111
Lawrence, C. R., Zucker, J. R., Readhead, A. C. S., et al. 1996, ApJS, 107, 541
Lehnert, M. D., & Becker, R. H. 1998, A&A, 332, 514
Lehnert, M. D., van Breugel, W. J. M., Heckman, T. M., & Miley, G. K. 1999, ApJS, 124, 11
Lin, H., Kirshner, R. P., Shectman, S. A., et al. 1996, ApJ, 464, 60
Magorrian, J., Tremaine, S., Richstone, D., et al. 1998, AJ, 115, 2285
Maraziti, D., & Stockton, A. 1994, PASP, 106, 71
Márquez, I., Durret, F., & Petitjean, P. 1999, A&AS, 135, 83
Márquez, I., Petitjean, P., Théodore, B., et al. 2001, A&A, 371, 97
McLeod, K. K., & McLeod, B. A. 2001, ApJ, 546, 782
McLeod, K. K., & Rieke, G. H. 1994, ApJ, 431, 137
McLeod, K. K., & Rieke, G. H. 1995, ApJ, 454, L77
McLure, R. J., Kukula, M. J., Dunlop, J. S., et al. 1999, MNRAS, 308, 377
Miller, P., Rawlings, S., & Saunders, R. 1993, MNRAS, 263, 425
Nolan, L. A., Dunlop, J. S., Kukula, M. J., et al. 2001, MNRAS, 323, 308
O'Dea, C. P., de Vries, W., Biretta, J. A., & Baum, S. A. 1999, AJ, 117, 1143
O'Dea, C. P., Stanghellini, C., Baum, S. A., & Charlot, S. 1996, ApJ, 470, 806
Örndahl, E., & Rönnback, J. 2003, in preparation (Paper II)
Poggianti, B. M. 1997, A&AS, 122, 399
Ridgway, S. E., Heckman, T. M., Calzetti, D., & Lehnert, M. 2001, ApJ, 550, 122
Romanishin, W., & Hintzen, P. 1989, ApJ, 341, 41
Rönnback, J., van Groningen, E., Wanders, I., & Örndahl, E. 1996, MNRAS, 283, 282 (R96)
Saglia, R. P., Bertschinger, E., Baggley, G., et al. 1993, MNRAS, 264, 961
Schade, D. J., Boyle, B. J., & Letawsky, M. 2000, MNRAS, 315, 498
Schlegel, D. J., Finkbeiner, D. P., & Davis, M. 1998, ApJ, 500, 525
Smith, E. P., Heckman, T. M., Bothun, G. D., Romanishin, W., & Balick, B. 1986, ApJ, 306, 64
Stockton, A., & MacKenty, J. W. 1987, ApJ, 316, 584
Stockton, A., & Ridgway, S. E. 2001, ApJ, 554, 1012
Tadhunter, C., Dickson, R., Morganti, R., et al. 2002, MNRAS, 330, 977
Tadhunter, C. N., Scarrott, S. M., Draper, P., & Rolph, C. 1992, MNRAS, 256, 53
Taylor, G. L., Dunlop, J. S., Hughes, D. H., & Robson, E. I. 1996, MNRAS, 283, 930
Urry, C. M., & Padovani, P. 1995, PASP, 107, 803
Vanden Berk, D. E., Richards, G. T., Bauer, A., et al. 2001, AJ, 122, 549
Városi, F., & Dwek, E. 1999, ApJ, 523, 265
Véron-Cetty, M. P., & Véron, P. 1993, ESO Sci. Rep., 13
Véron-Cetty, M.-P., & Woltjer, L. 1990, A&A, 236, 69
White, R. L., Becker, R. H., Gregg, M. D., et al. 2000, ApJS, 126, 133
Witt, A. N., & Gordon, K. D. 1996, ApJ, 463, 681
Witt, A. N., & Gordon, K. D. 2000, ApJ, 528, 799
Wold, M., Lacy, M., Lilje, P. B., & Serjeant, S. 2001, MNRAS, 323, 231